ScienSage

Journal of Advanced Scientific Research

Available online through http://www.sciensage.info

ISSN
0976-9595
Research Article

MOLECULAR IODINE CATALYZED SOLVENT FREE ONE POT SYNTHESIS, CHARACTERIZATION, *IN-SILICO* ADME, hERG ANALYSIS, MOLECULAR DOCKING STUDIES AND DFT ANALYSIS OF 2-SUBSTITUTED 4,5-DIPHENYL-1H-IMIDAZOLE DERIVATIVES

Pruthviraj K.[1], Lohith T. N.[2], Yeshwanth M.[3], Usha G. H.[1], Vanajakshi H. V.[1], Venugopal K. B.[1], Krishnaswamy G.[1], Shivaraja G.[1], Fathima Zohra[1], Sridhar M.A.[2], Sreenivasa S.*[1,4]

[1]*Department of Studies and Research in Organic Chemistry, Tumkur University, Tumakuru, Karnataka, India*

[2] *Department of Studies in Physics, Manasagangotri, University of Mysore, Mysuru, Karnataka, India*

[3] *Department of Biotechnology, Siddaganga Institute of Technology, Tumakuru, Karnataka, India*

[4] *Deputy Adviser, National Assessment and Accreditation Council, Nagarbhavi, Bengaluru, Karnataka, India*

**Corresponding author: drsreenivasa@yahoo.co.in*

ABSTRACT

In the present investigation, a series of 2-substituted 4,5-Diphenyl-1H-imidazoles (3a-f) were prepared via one pot Debus-Radziszwski multicomponent condensation reaction using molecular iodine as a catalyst. Synthesis involves one pot reaction of benzil and substituted aromatic aldehydes (2a-e) in the presence of ammonium acetate and molecular iodine as catalyst under the solvent free grinding technique. The structures of the compounds were established based on multi nuclear NMR (^{1}H &^{13}C) spectral data and mass spectrometry. These compounds were subjected to *in- silico* ADMETox evaluation, hERG analysis, and molecular docking studies to evaluate their potency as antibacterial, antifungal, anti-inflammatory, and antimycobacterial. Molecular physicochemical properties were analyzed using density functional theory (DFT), molecular electrostatic potential (MEP) studies and reduced density gradient analysis.

Keywords: 2-substituted 4,5-Diphenyl-1H-imidazole, *In silico* ADME, hERG, Molecular docking studies, DFT analysis, electrostatic potential.

1. INTRODUCTION

The discovery and development of compounds containing a large conjugated system with specific properties are of great interest in a multitude of areas of chemical research. Among which the Imidazole-based heterocyclic scaffolds play a vital role in natural and synthetic organic chemistry. The Imidazole or 1,3 diazole or glyoxaline based heterocycles play a vital role in natural and synthetic organic chemistry have been well exploited for many medicinal scaffolds exhibiting anti-HIV, anticancer, anticonvulsant, antifungal, antibacterial activities [1-8], and anti-tubercular [9,10]. A large number of imidazole-based compounds have been widely used as clinical drugs to treat various types of diseases with high therapeutic potency **(Fig. 1)**. These derivatives play a vital application in agrochemicals [11], dendrimers, polymers [12,13], plant growth regulators [14], TPFF sensors and fluorescent chemosensors [15-17], metal chelators [18], optical storage media and switches [19-21]. The most common method used for the synthesis of 2-Substituted 4,5-diphenyl-1H-imidazole derivatives bearing substituent at 2nd position is the Debus-Radziszewski multi component reaction (MCR) involving the condensation of benzil with different substituted benzaldehyde derivatives and ammonia in alcohol gives 2,4,5-triphenylimidazole (lophine). This reaction is the only reaction of industrial importance for the production of imidazole derivatives, the Radziszewski reaction has been further modified to proceed in the presence of Lewis acid as catalyst and ammonium acetate or ammonium carbonate as the source of nitrogen to give imidazoles with markedly improved yields [22-26]. The multicomponent reactions (MCRs) consist of two or more synthetic steps that are carried out without isolation of any intermediate. The development of MCRs in the presence of molecular iodine is an efficient approach that meets with the requirements of sustainable chemistry. Owing to numerous advantages associated with this eco-friendly

element, molecular iodine has been explored as a powerful catalyst for MCRs. The catalytic activity of molecular iodine is remarkable and the use of low cost, commercially available iodine as a catalyst for the synthesis of highly substituted imidazoles in excellent yields is also significant under the aspect of environmentally benign processes [27]. Therefore, we focused our interest on the synthesis of molecular iodine catalyzed solvent free one pot synthesis of 2,4,5-triarly-imidazole derivatives. Additionally, computer aided drug discovery approaches like ADMETox, hERG analysis and molecular docking studies were carried out. Results were compared with respective properties of extensively used antibacterial, antifungal, anti-inflammatory and antimycobacterial standard drugs ciprofloxacin **(CIP)**, clotrimazole **(CLO)**, indo-methacin **(IND)**, and ethambutol **(ETH)** respectively **(Fig.2)**. Finally, the synthesized compounds were subjected to DFT analysis, and MEP studies.

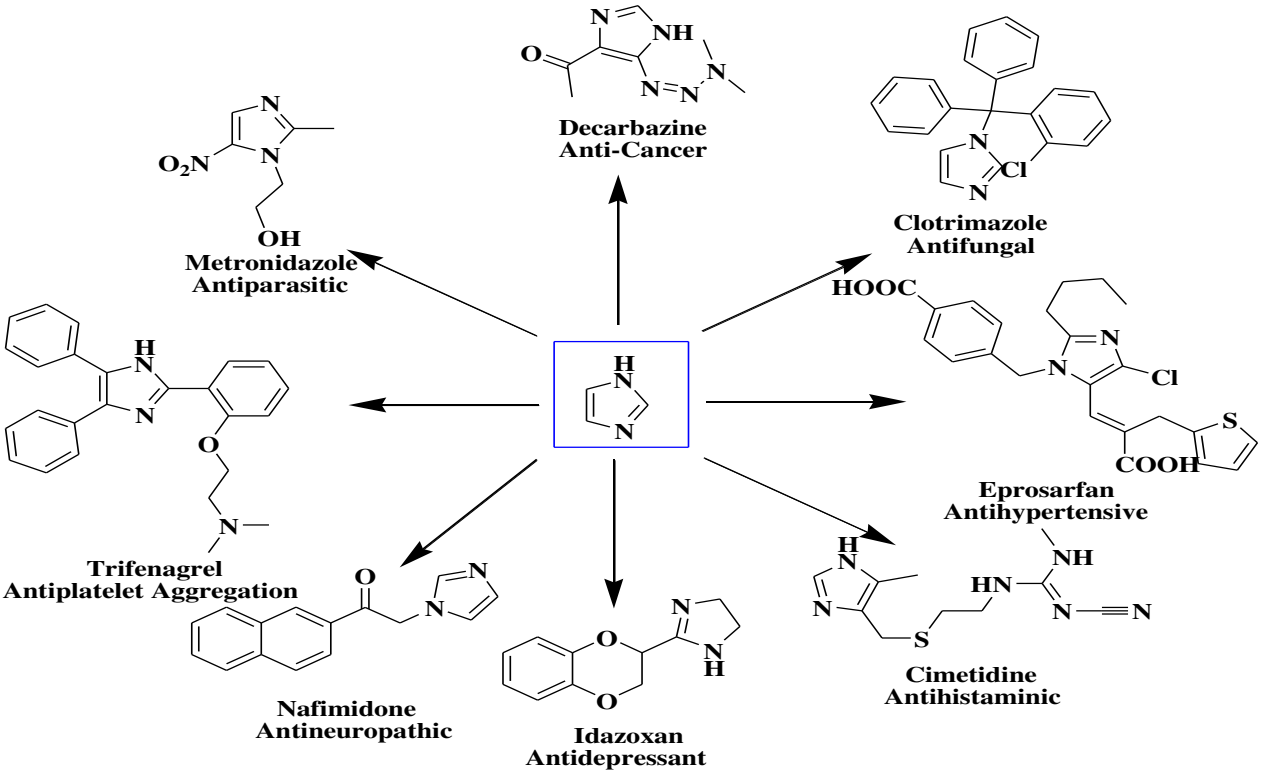

Fig. 1: Imidazole derivatized clinical drugs to treat various types of diseases

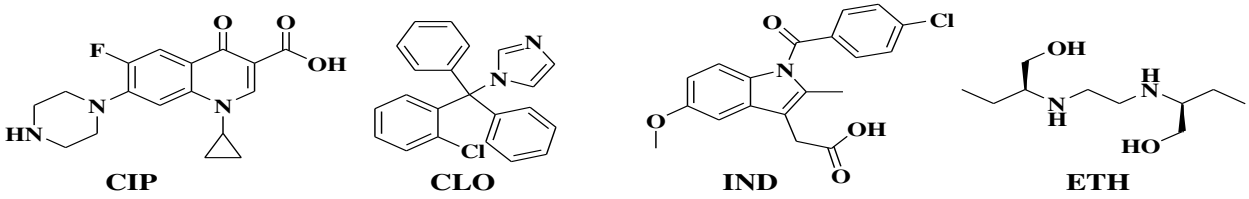

Fig. 2: Standard antibacterial, antifungal, anti-inflammatory and antimycobacterial drugs

2. MATERIAL AND METHODS

The organic solvents and chemicals purchased from Merck, Spectrochem, Sigma Aldrichand standard commercial sources,were used without further purification. Melting point ranges of solid compounds were determined in open capillary tubes using a hot stage apparatus. Progress of the reactions was monitored by TLC using Merck silica gel 60 F_{254} precoated on aluminium backed plates. ^{1}H and ^{13}CNMR spectra were recorded on Varian NMRS 400 Agilent at 400MHz, and ECX500 Jeol 400 MHz high resolution multinuclear FT NMR Spectrometer with LN_2 cooled probe using deuterated solvents ($CDCl_3$ or DMSO-d_6), chemical shifts were expressed in parts per million

(ppm) and Tetramethylsilane (TMS) as an internal standard. The Mass spectra were recorded using waters alliance 2795 separation module and the waters micromass LCT mass detector.

2.1. Experimental

2.1.1. General procedure for the synthesis of 2-Substituted 4,5-Diphenyl-1H-Imidazole-derivatives (3a-f)

A mixture of different substituted aldehydes (1mmol), benzil (1mmol), NH_4OAC (1mmol) and molecular iodine (5mol%), were ground together in a mortar with a pestle at room temperature for an appropriate time (30 min to 1 hr). The reaction was monitored by thin layer chromatography using 7:3 n-hexane-ethyl acetate solvent system. After the completion of the reaction, the mixture was treated with aqueous sodium thiosulfate ($Na_2S_2O_3$) to furnish the solid crude product, filtered and washed with water. The pure compounds were obtained through recrystallization using ethanol [28].

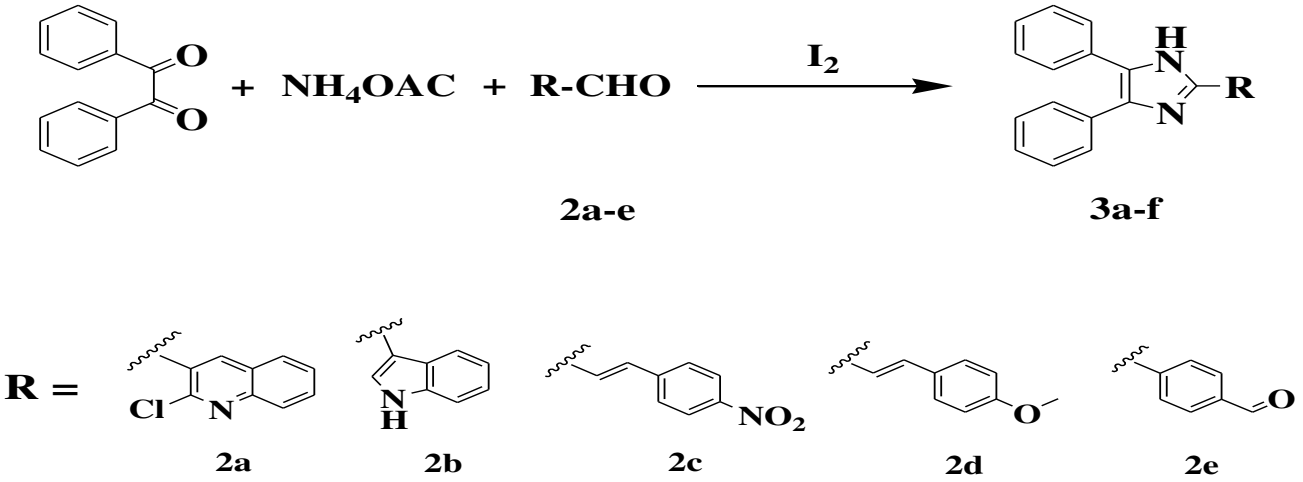

Scheme 1: Synthetic route for the preparation of 2-Substituted 4,5-Diphenyl-1H-Imidazole-derivatives(3a-f) via one pot molecular iodine catalyzed grinding technique.

3. RESULTS AND DISCUSSION

3.1. Chemistry

2-Substituted-4,5-Diphenyl-1H-imidazole derivatives **(3a-f)** were synthesized by the reaction of benzyl with different substituted aldehydes **(2a-e)** in the presence of molecular iodine as a catalyst at lab temperature using solvent free grinding technique and ammonic acetate as a source of nitrogenas depicted in **Scheme1**.The assigned structures of the imidazole derivatives were confirmed by their physicochemical parameter (**Table1)** and spectral studies (multi nuclear NMR (^1H &^{13}C) and Mass analysis).

The structure of all the synthesized lophine derivatives **(3a-f)**were ascertained using melting point (mp), mass spectrometry (LC-MS), ^1H and ^{13}C Nuclear magnetic resonance (NMR) spectral data. The results were good and are in agreement with the previous literature reports **(3a, 3b, 3e & 3f).** Affirmatively, ^1H and ^{13}C NMR spectral analysis were done. The NMR chemical shift of the N-H proton of imidazole ring was observed at δ 12 ppm. The peaks in the range of δ 6.8-8.0 ppm were attributed to the C-5, C-4 phenyl ring, and C-2 bearing substituent protons of imidazole moiety. Due to the complex nature of NMR, the splitting pattern was not clear for these derivatives. In ^{13}C NMR spectra, the peaks at around 120-140 ppm for the aromatic carbons of the derivatives and the peak above 140 ppm for C-2 carbon of imidazole ring confirmed all synthesized derivatives. M+1 peak of LC-MS spectra also added evidence to the product formation.

3.1.1. Possible Mechanism

Molecular iodine catalyzes the reaction as a mild Lewis acid. Molecular iodine is capable of bonding with the carbonyl oxygen increasing the reactivities of the parent carbonyl compounds. Iodine facilitates the formation of a diamine intermediate (I), which under mild acid catalysis of iodine condenses further with the carbonyl carbon of 1,2 diketone followed by dehydration to afford the iso-imidazole (II), which rearranges via [1,5] sigmatropic shift to the required imidazoles **(Fig. 3)**.

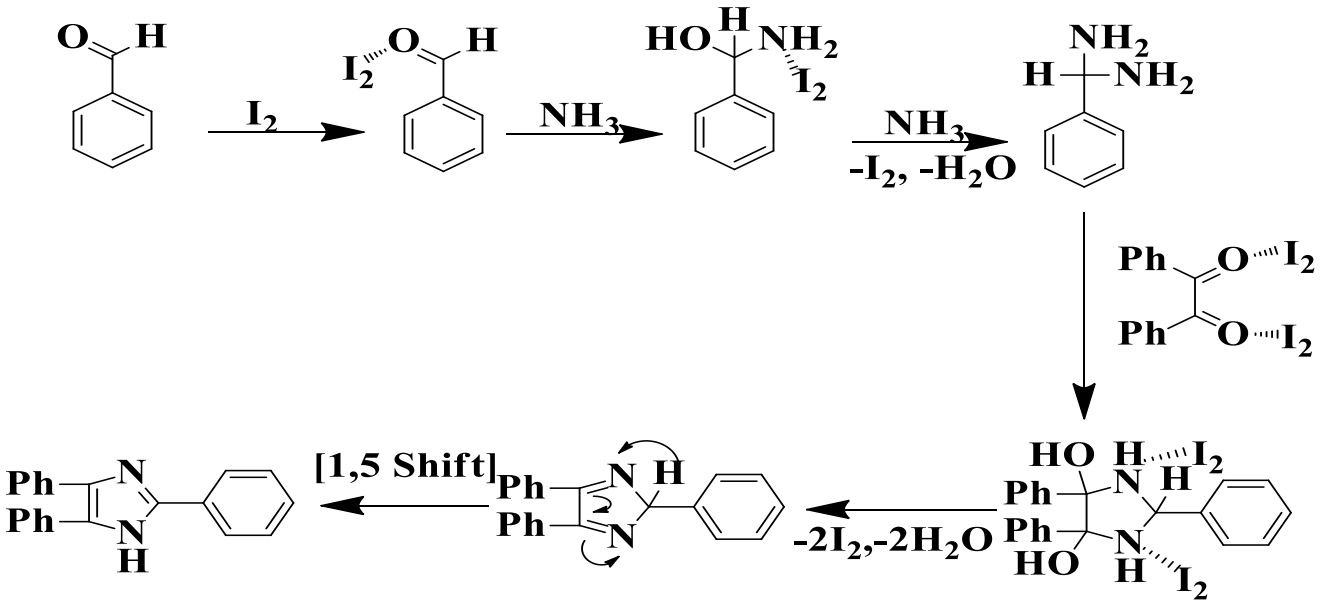

Fig. 3: Possible Mechanism for the formation of 2-Substituted 4,5-Diphenyl-1H-Imidazole derivatives (3a-f)

Table 1: Physical characterization data of synthesized compounds

Code	Molecular Formula	Molecular weight	Color	mp(°C) (Found)	mp(°C) (Literature)	% Yield
3a	$C_{24}H_{16}ClN_3$	381.86	Yellow Crystal	201-203	205-207 [29]	92
3b	$C_{23}H_{17}N_3$	337.42	Brown Solid	292-293	290-291 [30]	95
3c	$C_{23}H_{17}N_3O_2$	367.40	Orange solid	>300	-	88
3d	$C_{24}H_{20}N_2O$	352.43	Brown solid	248-252	-	82
3e	$C_{22}H_{16}N_2O$	324.38	Off white solid	238-240	240-242 [31]	82
3f	$C_{36}H_{26}N_4$	514.62	Light yellow Crystal	230-232	232-235 [32]	95

3.1.2. 2-Chloro-3-(4,5-diphenyl-1H-imidazol-2-yl)quinoline(3a):

^{1}H NMR (400MHz,DMSO-d_6, δ ppm): 12.20 (br s, 1H, NH), 8.79 (s, 1H,ArH), 8.79-7.26 (m, 14H, ArH).**^{13}C NMR (100MHz,DMSO-d_6, δ ppm):** 160.93, 142.27, 137.88, 137.35, 135.41, 134.88, 130.08, 130.70, 128.83, 128.60, 128.24, 127.76, 127.37, 127.03, 126.87, 122.70, 119.73, 119.36, 115.25.**MS:** Calculated - 381.1; Observed- (M+1) - 382.2.

3.1.3. 3-(4,5-Diphenyl-1H-imidazol-2-yl)-1H-indole(3b):

^{1}H NMR (400MHz,DMSO-d_6, δ ppm): 12.50 (s, 1H, NH) 11.61(s, 1H), 7.11-8.49 (m, 15H, ArH).**^{13}C NMR (100MHz,DMSO-d_6, δ ppm):** 143.86, 136.33, 135.58, 129.62, 129.54, 128.16, 126.97, 126.17, 125.13, 123.98, 121.50, 119.62, 111.65, 106.79.**MS:**Calculated=335.1; Observed-(M+1)- 336.2.

3.1.4. 2-(4-Nitrostyryl)-4,5-diphenyl-1H-imidazole(3c):

^{1}H NMR (400MHz, DMSO-d_6, δ ppm): 6.719-6.761 (s, 2H, HC=CH) 7.561-8.080 (m, 14H, ArH) 12.818 (s,1H, NH). **^{13}C NMR (100MHz, $CDCl_3$, δ ppm):** 123.821, 124.000, 127.5 128.039, 128.720, 129.167, 129.3, 130.043, 133.147, 135.034, 136.2, 138.200, 143.007, 147.001. **MS:** Calculated- 367.4; Observed-(M+1)- 367.5.

3.1.5. 2-(4-methoxystyryl)-4,5-diphenyl-1H-imidazole(3d):

^{1}H NMR (400MHz, $CDCl_3$, δ ppm): 3.722(s, 3H,-OCH3) 6.226-6.268 (s, 2H, HC=CH) 7.445-8.501(m, 14H, ArH) 12.732 (s,1H, NH).**^{13}C NMR (100MHz, $CDCl_3$, δ ppm):** 55.459, 114.398, 114.671, 124.0, 128.039, 128.720, 129.167, 129.8, 130.043, 133.147, 135.034. 138.2, 159.8. **MS:** Calculated- 352.1; Observed- (M+1) - 352.3.

3.1.6. 4-(4,5-diphenyl-1H-imidazol-2-yl) benzaldehyde(3e):

^{1}H NMR (400MHz, $CDCl_3$, δ ppm): 7.260-8.055 (m, 14H, ArH) 10.013(s, 1H, -CHO) 12.651 (s,1H, NH).**^{13}C NMR (100MHz,DMSO-d_6, δ ppm):** 123.512, 129.337, 129.536, 129.627, 130.027, 132.221, 135.588, 138.023, 192.937, 194.848.**MS:** Calculated- 324.4; Observed- (M+1) - 325.4.

3.1.7. 1,4-bis(4,5-diphenyl-1H-imidazol-2-yl) benzene(3f):

^{1}H NMR (400MHz, DMSO-d_6, δ ppm): 7.23-8.18 (m, 24H, ArH) 12.75 (s, NH).**^{13}C NMR (100MHz, DMSO-d_6, δ ppm):** 125.37, 126.58, 127.09, 127.82, 128.19, 128.40, 128.66, 130.98, 135.10, 145.14.**MS:** Calculated- 514.1; Observed- (M+1)- 515.2.

3.2. ADMETox evaluation

By applying computational methods, various physico-chemical features and pharmacokinetic descriptors and *in silico* toxicity evaluations were evaluated through the online web tool Swiss ADME (http://www.swissadme.ch/) [33] and ADMET Lab (http://admet.scbdd.com/calcpre/index_sys/) [34], to predict ADME and toxicity values for derivatives **(3a-f)** prepared.

3.2.1. Molecular parameters, drug-likeness, bio-availability and synthetic accessibility

For a compound to be orally bioavailable in terms of molecular and pharmaceutical properties like solubility, chemical stability, bioavailability, and distribution profile having zero or negative value should not be considered as drug-like [35]. Exploration of *in silico* ADME properties of synthesized compounds in terms of molecular properties showed that compound **(3a)**and **CLO** violated MlogP>4.15 and remaining compounds **(3b-f)**were found in good agreement with Lipinski's rule of five.

Further, synthetic accessibility of the compound **(3a-f)** along with standard drugs **CIP, CLO, IND, ETH** was determined to quantify the complexity of the molecular structure. The results showed that the score was in the range of 2.40-3.25 revealed that the compounds and standard drugs do not have a complex synthetic route as tabulated in (**Table2)**.

Table 2: Physiochemical parameters, bioavailability and synthetic accessibility of compounds

Code	Molecular Weight	Mlog P	nHBA	nHBD	nRB	TPSA (Å)	nViolations	Bioavailability Score	Synthetic accessibility
3a	381.86	4.28	2	1	3	41.57	1	0.55	3.13
3b	335.40	3.63	1	2	3	44.47	0	0.55	2.97
3c	367.40	3.98	3	1	5	74.50	0	0.55	3.25
3d	352.43	3.64	2	5	1	37.91	0	0.55	3.14
3e	324.38	3.22	2	1	4	45.75	0	0.55	2.78
3f	514.62	5.27	2	2	6	57.36	2	0.17	3.81
CIP	331.34	1.28	5	2	4	74.57	0	0.55	2.51
CLO	344.84	4.38	1	0	4	17.82	1	0.55	2.70
IND	357.79	3.30	4	1	5	68.53	0	0.56	2.51
ETH	204.31	0.18	9	4	4	64.52	0	0.55	2.40

nHBA: Hydrogen bond acceptor, nHBD: Hydrogen bond donor, MW: Molecular weight, Alogp: logarithm of partition between n-octanol and water, nRB: Number of rotatable bonds, TPSA: Topological polar surface area.

The drug-likeness scores were also calculated by considering (mLogP, TPSA, nAtoms, nON, nOHNH, rotb and MW) based on Lipinski's, Ghose and Veber rule for the prediction of bioactivity scores. The results of these showed that the compounds obeyed Lipinski's, Ghose and Veber rule except compound **(3a&3f)** and **CLO** which violates Lipinski's rule (**Table3**).

The compound's aqueous and non-aqueous solubility influences the absorption and is an important factor in view of the drug development process. High water solubility of drugs is important to deliver active ingredient and to estimate **log S** scale was used: if log S <10 μg/mL: low solubility; 10-60 μg/mL: moderate solubility; >60 μg/mL: high solubility. Based on these predictive models, compounds **(3a), (3c)**and **(3e)** were predicted to be poorly soluble, while compounds **(3b), (3d), (3f), CLO,** and **IND** were predicted to be moderately soluble and **CIP, ETH** was highly soluble.

LogD(distribution coefficient D): **<1:** solubility high; permeability low by passive trans-cellular

diffusion; permeability possible via para-cellular if MW < 200; metabolism low.

1 to 3: solubility moderate; permeability moderate; metabolism low.

3 to 5: solubility low; permeability high; metabolism moderate to high.

> 5: solubility low; permeability high; metabolism high.

LogP (distribution coefficient P) ranges optimal: **0<LogP<3;<0:** poor lipid bilayer permeability;**>3:** poor aqueous solubility as tabulated in **(Table4)**.

Table 3: Drug likeness, bioactivity score and synthetic accessibility of the compounds

Code	Drug likeness										
	Lipinski					Ghose			Veber		
	MW ≤ 500	Mlog P ≤ 4.15	N or O≤10	NH or OH ≤ 5		160 ≤ MW ≤ 480	20 ≤ atoms ≤70		Rotatable bonds≤10	TPSA ≤140	
3a	381.86	4.28	2	1	N(1)	381.86	28	Y	3	41.57	Y
3b	335.40	3.63	1	2.	Y	335.40	26	Y	3	44.47	Y
3c	367.40	3.78	3	1	Y	367.40	28	Y	5	74.50	Y
3d	352.43	3.64	2	1	Y	352.43	27	Y	5	37.91	Y
3e	324.38	3.22	2	1	Y	324.38	25	Y	4	45.75	Y
3f	514.62	5.27	2	2	N(2)	514.62	40	N(1)	6	57.36	Y
CIP	331.34	1.28	5	2	Y	331.34	24	Y	3	74.57	Y
CLO	344.84	4.38	1	0	N(1)	344.84	25	Y	4	17.82	Y
IND	357.79	3.30	4	1	Y	357.79	25	Y	5	68.53	Y
ETH	204.31	0.18	4	4	Y	204.31	14	Y	9	64.52	Y

Table 4: Predicted solubility parameters in ADME of compounds

Code	LogS (solubility) ug/ml	LogD (distribution coefficient D)	LogP (distribution coefficient P)	Solubility class
3a	0.158	3.396	6.13	Poorly soluble
3b	0.429	3.415	4.928	Moderate soluble
3c	0.034	3.119	5.34	Poorly soluble
3d	0.061	2.09	5.441	Moderate soluble
3e	1.592	3.192	4.741	Moderate soluble
3f	0.651	3.536	8.171	Poorly soluble
CIP	171.903	-0.705	1.583	Very soluble
CLO	0.061	3.119	5.377	Moderate soluble
IND	3.004	0.663	3.927	Moderate soluble
ETH	50617.2	0.075	-0.293	Very soluble
Standard	**>10**	**1 to 5**	**0 to 3**	

The brain or intestinal estimated permeation method (BOILED-Egg) (**Fig. 4** & **5**) was proposed as an accurate predictive model that works by computing the lipophilicity and polarity of small molecules. The white region indicates passive gastrointestinal (GI) absorption and the yellow region indicates passive brain permeation. All the synthesized derivatives and standards have high GI absorption, except **ETH** with moderate **(Table 5)**. While all derivatives including standards **CLO** & **IND** have BBB permeant and hence there is possibility of causing harmful effect on brain and blood stream when metabolized as tabulated in **(Table 6)**. The remaining standards **CIP** & **ETH** were predicted to be non-blood-brain penetrates. A molecule is said to be less skin permeant if the value of log Kp is more negative. From the predicted results, all the compounds **(3a-f)** and standards **CLO & IND** were found to be the least skin permeant **(Table 5)**, further PPB (Plasma Protein Binding): significant with drugs that are highly protein-bound and have a low therapeutic index**. VD (volume distribution)**: Optimal: 0.04-20L/kg; Range:<0.07L/kg: Confined to blood, Bound to plasma protein or highly hydrophilic; 0.07-0.7L/kg: Evenly distributed; > 0.7L/kg: Bound to tissue components (e.g., protein, lipid), highly lipophilic **(Table 6)**.

Metabolism plays important role in the bioavailability of drugs as well as drug-drug interactions. It is also important to have a better understanding if a certain compound is a substrate or non-substrate of the certain proteins. The permeability glycoprotein **(P-gp)** is an important protein in assessing active efflux through

biological membranes and cytochrome P450 **(CYP)** enzymes. Hence, the compounds were evaluated to determine whether they can act as a substrate or an inhibitor of **P-gp** and **CYP**s. Compounds **(3a), (3c), (3d),(3e)** and **IND** were found to be P-gp inhibitor **(Table 5).** The CYPS substrate or inhibitor properties and elimination parameter were tabulated in (**Table 7)** and (**Table8)** respectively.

Table 5: Predicted absorption parameters in ADME of compounds

Code	Papp (Caco-2 Permeability, cm/s	Pgp-inhibitor	Predicted Value	Pgp-substrate	Predicted Value	HIA (Human Intestinal Absorption)	Predicted Value	Log Kp (cm/s)
3a	-4.747	Y	0.613	N	0.016	High	0.895	-4.17
3b	-4.964	N	0.493	N	0.104	High	0.833	-4.68
3c	-5.004	Y	0.828	N	0.022	High	0.816	-4.62
3d	-4.955	Y	0.919	N	0.037	Very high	0.799	-4.43
3e	-4.876	Y	0.673	N	0.055	Very high	0.91	-5.08
3f	-5.135	N	0.218	N	0.06	High	0.855	-3.64
CIP	-5.165	N	0.329	Y	0.839	High	0.819	-9.09
CLO	-4.567	N	0.095	Y	0.549	High	0.895	-4.56
IND	-4.744	Y	0.683	N	0.031	High	0.785	-5.45
ETH	-5.545	N	0.028	N	0.138	Moderate	0.664	-7.70

Table 6: Predicted distribution parameters in ADME of compounds

Code	PPB (Plasma Protein Binding %)	VD (Volume Distribution) L/kg	BBB Permeability	Predicted Value
3a	78.23	0.368	High	0.879
3b	77.161	0.964	Very high	0.983
3c	88.47	-0.195	Very high	0.913
3d	92.64	0.503	Very high	0.939
3e	82.138	0.394	Very high	0.91
3f	73.78	0.262	Very high	0.971
CIP	69.358	0.503	No	0.043
CLO	61.985	0.663	Very high	0.985
IND	94.527	-1.058	High	0.785
ETH	29.783	0.329	No	0.047
Standard	90	0.04~20 L/kg	----	----

Table 7: Predicted metabolism parameters in ADME of compounds

Code	CYP1A2 inhibitor	Predicted Value	CYP1A2 Substrate	Predicted Value	CYP3A4 inhibitor	Predicted Value	CYP3A4 substrate	Predicted Value	CYP2C9 inhibitor	Predicted Value
3a	Y	0.98	Y	0.64	Y	0.589	N	0.398	Y	0.717
3b	Y	0.952	Y	0.674	Y	0.698	N	0.341	Y	0.612
3c	Y	0.758	Y	0.682	N	0.428	N	0.37	N	0.417
3d	Y	0.947	Y	0.688	Y	0.74	N	0.462	N	0.442
3e	Y	0.967	Y	0.62	N	0.233	N	0.316	N	0.184
3f	Y	0.982	Y	0.688	N	0.108	N	0.274	N	0.08
CIP	N	0.031	Y	0.544	N	0.043	N	0.29	N	0.1
CLO	Y	0.968	Y	0.628	Y	0.931	N	0.168	Y	0.957
IND	N	0.307	Y	0.56	N	0.113	Y	0.52	N	0.367
ETH	N	0.02	N	0.482	N	0.01	N	0.28	N	0.012

Code	CYP2C9 substrate	Predicted Value	CYP2C19 inhibitor	Predicted Value	CYP2C19 substrate	Predicted Value	CYP2D6 inhibitor	Predicted Value	CYP2D6 substrate	Predicted Value
3a	N	0.454	Y	0.705	N	0.336	N	0.336	N	0.43
3b	N	0.477	N	0.391	N	0.91	Y	0.515	N	0.44
3e	Y	0.527	Y	0.54	N	0.387	N	0.387	N	0.353
3f	Y	0.653	Y	0.602	Y	0.602	N	0.459	Y	0.631
3e	Y	0.515	N	0.457	N	0.402	N	0.335	N	0.394
3f	N	0.4	N	0.344	N	0.4	N	0.335	N	0.414
CIP	N	0.069	N	0.075	N	0.314	N	0.188	N	0.042
CLO	N	0.204	Y	0.841	Y	0.571	Y	0.877	N	0.113
IND	Y	0.963	N	0.217	Y	0.838	N	0.225	N	0.269
ETH	N	0.404	N	0.014	N	0.312	N	0.218	Y	0.525

Table 8: Predicted elimination parameters in ADME of compounds

Code	$T_{1/2}$(Half Life Time) h	CL (Clearance Rate) mL/min/kg
3a	2.285	1.678
3b	2.348	2.108
3c	2.044	1.233
3d	2.022	1.965
3b	2.348	2.108
3a	2.285	1.678
CIP	1.857	1.316
CLO	2.483	1.239
IND	1.632	1.297
ETH	1.318	2.064
Stad	> 0.5	-

$T_{1/2}$ (Half Life Time):Range: >8h: high; 3h< Cl < 8h: moderate; <3h: low, CL (Clearance Rate):Range: >15 mL/min/kg: high; 5mL/min/kg< Cl < 15mL/min/kg: moderate; <5 mL/min/kg: low

Toxicity evaluation is initially used to determine the compound's toxicity as a fast and inexpensive method. The Median lethal dose (LD_{50}) usually represents the acute toxicity of chemicals. It is the dose amount of a tested molecule to kill 50 % of the treated animals within a given period. Here, the synthesized compounds **(3a-f)** were subjected to an *in silico* toxicity evaluation. The toxicity class ranges from 1 to 6 as shown below

Class I: fatal if swallowed ($LD_{50} \leq 5$)
Class II: fatal if swallowed ($5 < LD_{50} \leq 50$)
Class III: toxic if swallowed ($50 < LD_{50} \leq 300$)
Class IV: harmful if swallowed ($300 < LD_{50} \leq 2000$)
Class V: may be harmful if swallowed ($2000 < LD_{50} \leq 5000$)
Class VI: non-toxic ($LD_{50} > 5000$)

The results showed that the synthesized compounds **(3a-f)**, **CIP** and **CLO** were predicted to be harmful if swallowed and belongs to class 4. **IND** was predicted to be toxic if swallowed belongs to class 3 and **ETH** was predicted may be harmful if swallowed and belongs to class 5 (**Table9**) and further toxicity endpoints are listed in (**Table 10)**.

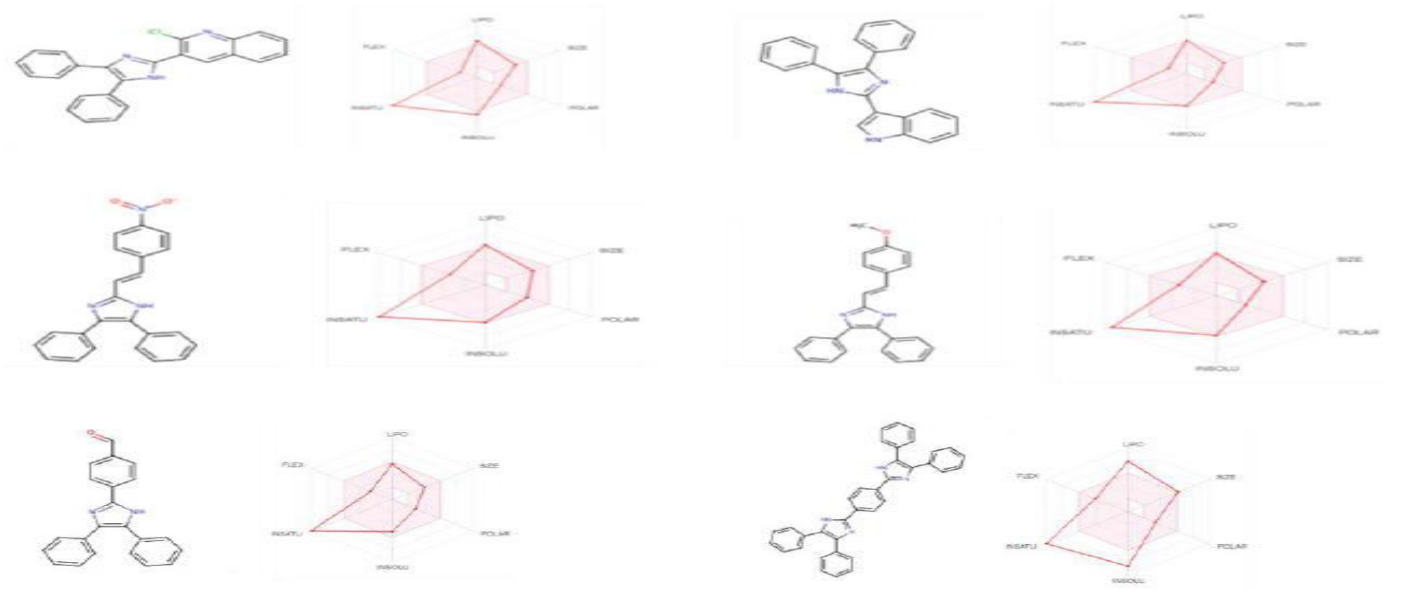

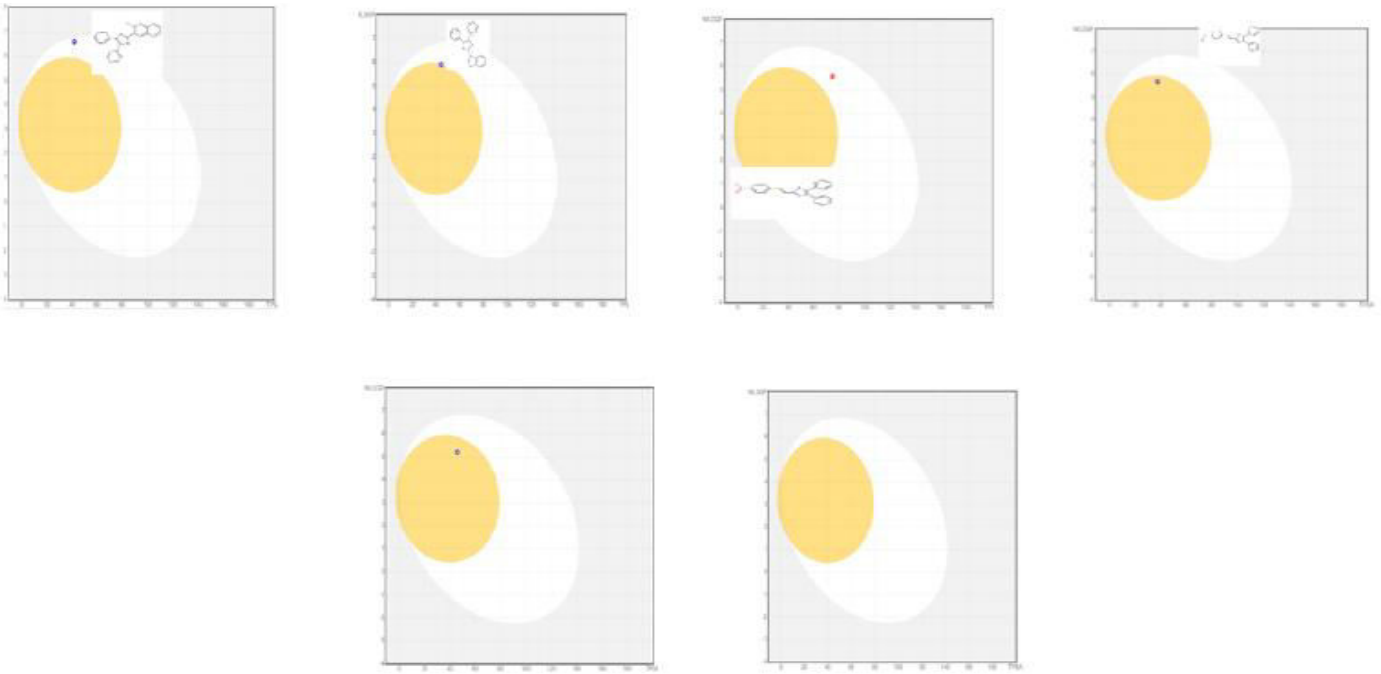

Fig. 4: 2D structure, bioavailability radar and boiled egg images of compounds 3a-f

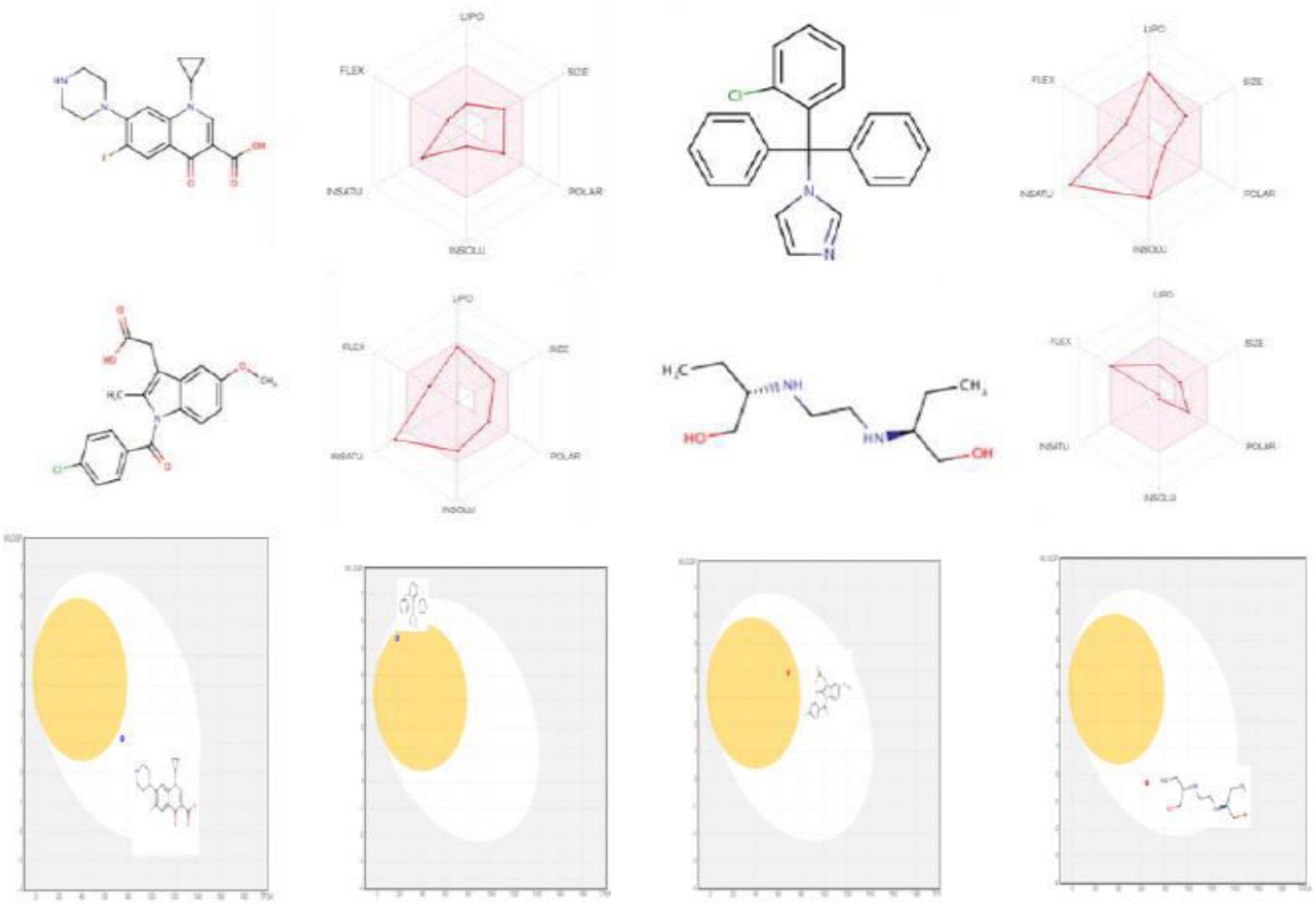

Fig. 5: 2D structure, bioavailability radar and boiled egg images of standard drugs CIP,CLO,IND & ETH

Table 9: Predicted LD_{50} and Toxicity class of the compounds

Code	LD50 (LD50 of acute toxicity) mg/kg	Toxicity Class	DILI (Drug Induced Liver Injury)	Predicted Value	MDD (Maximum Recommended Daily Dose)	Predicted Value
3a	1207.566	IV	High	0.782	No	0.488
3b	836.641	IV	High	0.828	Moderate	0.536
3c	1191.65	IV	High	0.82	Moderate	0.584
3d	855.227	IV	High	0.784	Moderate	0.5
3e	822.353	IV	High	0.838	Moderate	0.566
3f	773.565	IV	High	0.768	Moderate	0.614
CIP	1089.64	IV	Very High	0.994	High	0.804
CLO	766.697	IV	Moderate	0.63	Moderate	0.63
IND	106.569	III	Very High	0.936	Moderate	0.584
ETH	2164.204	V	No	0.08	High	0.888
Standard	>500		High	0.782	No	0.488

Table 10: Predicted activity of the compounds on toxicity endpoints

Code	hERG (hERG Blockers)	Predicted Value	H-HT (Human Hepatotoxicity)	Predicted Value	AMES (Ames Mutagenicity	Predicted Value	SkinSen (Skin sensitization)	Predicted Value
3a	High	0.835	High	0.78	Moderate	0.508	No	0.467
3b	High	0.846	High	0.66	Moderate	0.64	No	0.46
3c	High	0.822	High	0.7	High	0.882	Moderate	0.616
3d	High	0.902	High	0.842	High	0.866	No	0.402
3e	High	0.846	Moderate	0.66	Moderate	0.64	No	0.46
3f	High	0.835	High	0.78	Moderate	0.508	No	0.467
CIP	No	0.418	Very High	0.97	Moderate	0.646	No	0.328
CLO	High	0.886	High	0.894	Moderate	0.294	Moderate	0.594
IND	High	0.767	High	0.968	No	0.222	No	0.167
ETH	No	0.161	High	0.736	No	0.06	Moderate	0.669

3.3. hERG analysis

The blockage of the hERG K+ channels is closely associated with lethal cardiac arrhythmia. The notorious ligand promiscuity of this channel earmarked hERG as one of the most important anti targets to be considered in the early stages of the drug development process. Since several non-cardiovascular drugs exhibited lethal hERG K+ channel blocking ability its necessary to find out that hERG anti-target at the early stages of drug development. Using online web tool Pred-hERG4.2 (http://predherg.labmol.com.br/) [36] derivatives **(3a-f) (Fig. 6** & **table 11)** were screened for their hERG anti-target. In the map, green atoms or fragments represent contribution towards blockage of hERG, while pink means that it contributes to a decrease of hERG blockage, and gray means no contribution. Gray iso-lines delimit the region of the split between the positive (green) and the negative (pink) contribution.

3.4. Molecular Docking Studies

In-silico molecular docking is a computational technique in the rational design of drugs and is widely used to predict the binding orientation of small molecule drug candidates to protein targets in order to predict the affinity and activity of the small molecule. Molecular docking analysis was performed to predict the mechanism of action. The molecule with the lowest binding energy tends to have the highest binding affinity to the target protein.

3.4.1. Preparation of Ligands

The molecule structures were generated based on spectral data multi nuclear NMR (1H & 13C) and Mass Spectrometry. These structures were drawn in Marvin JS software (https://marvinjs-demo.chemaxon.com/latest/demo.html) and they were cleaned & orientated to 3D. All these structures of the molecule were prepared in Auto Dock 4.2 software and exported into pdbqt file format.

Table 11: Predicted activity hERG blocker of compounds 3a-f

Code	hERG Blockers	Probability	Potency	% Confidence
3a	High	0.835	Potential Cardiotoxic	60
3b	High	0.846	Potential Cardiotoxic	70
3c	High	0.822	Potential Cardiotoxic	60
3d	High	0.902	Potential Cardiotoxic	60
3b	High	0.85	Potential Cardiotoxic	50
3a	High	0.775	Potential Cardiotoxic	60
CIP	No	0.418	No Cardiotoxic	90
CLO	High	0.886	Potential Cardiotoxic	80
IND	High	0.767	No Cardiotoxic	80
ETH	No	0.161	No Cardiotoxic	60

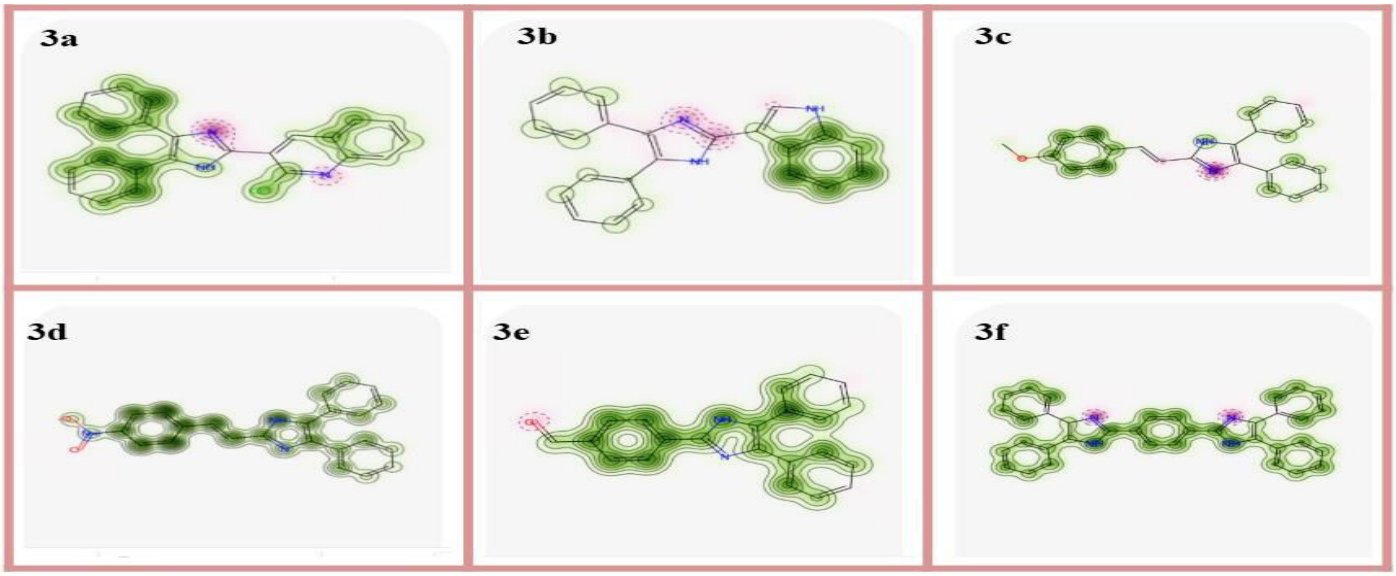

Fig. 6: hERG blocking diagram of compounds 3a-f

3D Structures of Antibacterial target protein *Dehydroqualene synthase of S. aureus* with PDB ID 3ACX, Antimycobacterial Protein target: *Mycobacterium tuberculosis Enoyl reductase* with PDB ID: 4TZT, Anti-fungal Protein target: *Candida albicans N-myristoyl transferase* with PDB ID: 1IYL, and Anti-inflammatory Protein target: *Aspirin acetylated cyclooxygenase-1*with PDB ID: 3N8Y were chosen from the Protein Data Bank (PDB), website www.rcsb.org. Water molecules and metal ions were removed from the protein structures to obtain clean protein. The protein thus obtained was subjected to energy minimization in DS 3.1 using the CHARMm force field. The CHARMm force energy was fixed to (0.001 kcal/mole) and minimized for docking and simulations. The active site was defined from the collection of residues within 10.0 Å of the bound inhibitor that comprised the union of all ligands of the ensemble. All atoms located less than 10.0 Å from any ligand atom were considered.Based on docking the top 10 poses will be generated and ranked based on binding energy. The docking results for receptor ligand complex comprised of intermolecular interaction energies namely hydrogen bonding, hydrophobic and electrostatic interactions are presented in Receptor-ligand complex with the least binding energy was used to infer the best binding molecule in the series of the tested Compounds. The best conformations were selected based on the least docking energy value, several ligand conformations were obtained based on CHARM energy, bond energy, initial potential energy, dihedral energy, electrostatic energy and initial RMS gradient values. The drug characteristics were evaluated using the Lipinski rule of 5 [37]. 2D docking poses are shown in the antibacterial **(Fig.7)**, antimycobacterial **(Fig.8)**, antifungal **(Fig. 9)**, and anti-inflammatory (**Fig.10),** binding/docking energy values are tabulated in the **Table 12.**

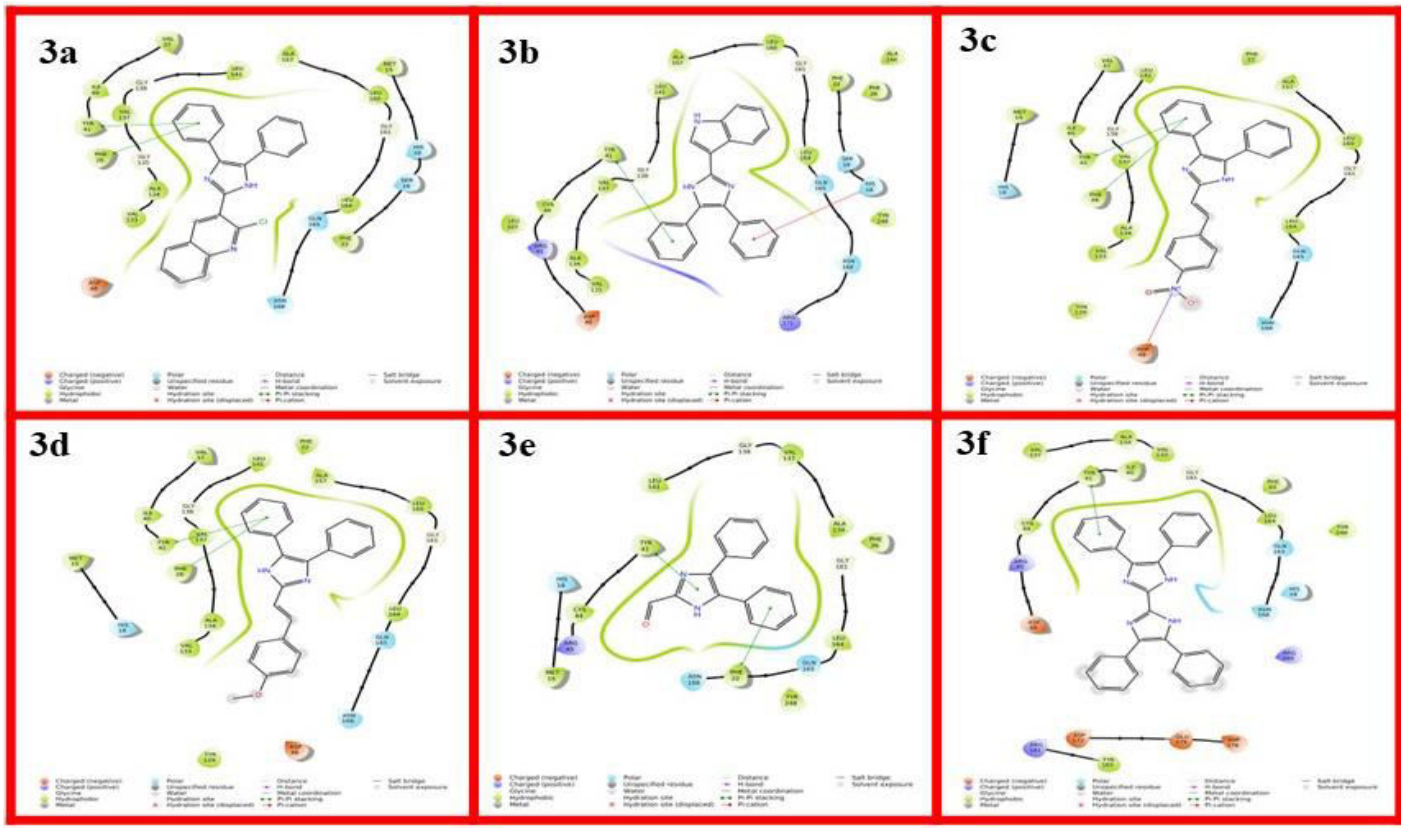

Fig. 7: Antibacterial docking poses of compounds 3a-f

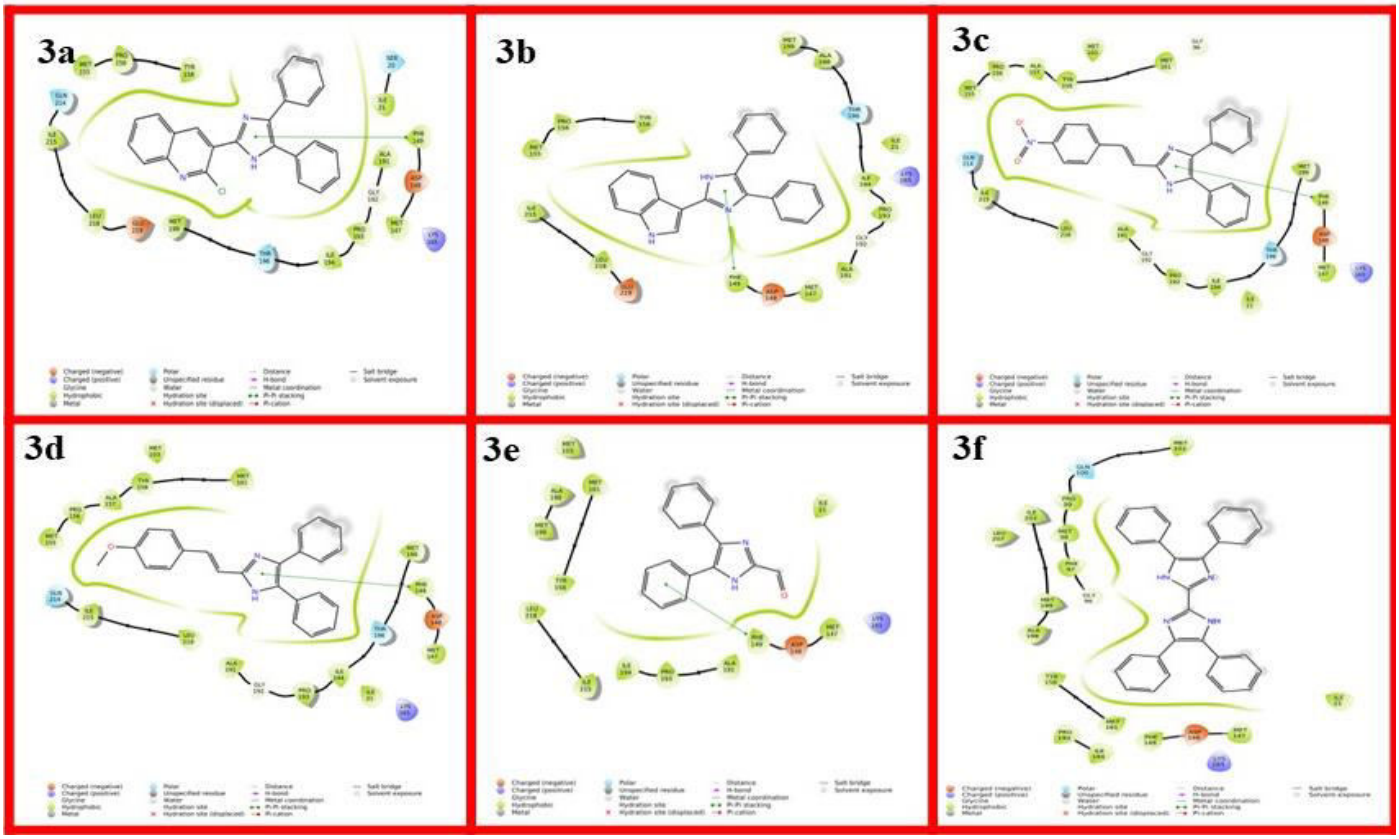

Fig. 8: Anti-mycobacterial docking poses of compounds 3a-f

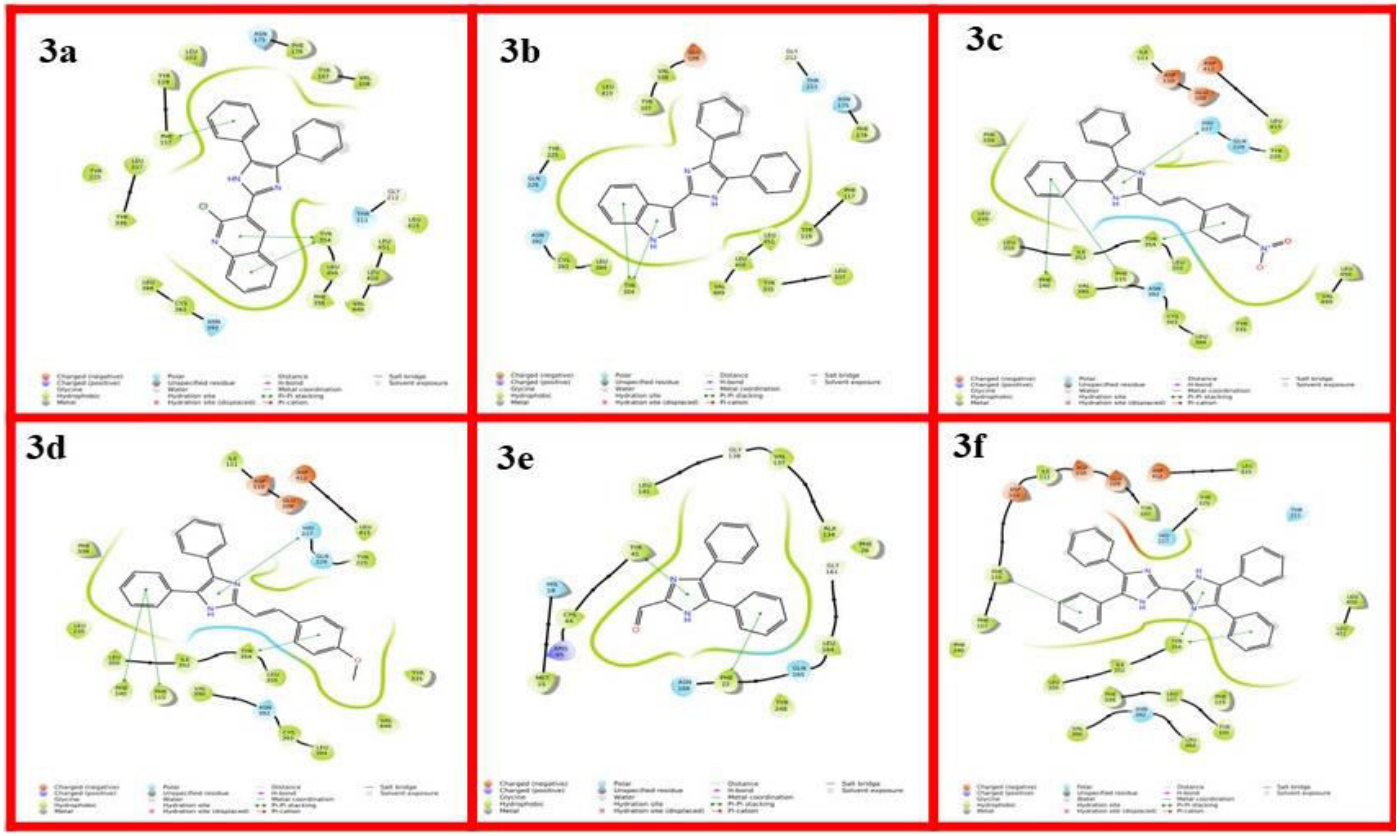

Fig. 9: Antifungal docking poses of compounds 3a-f

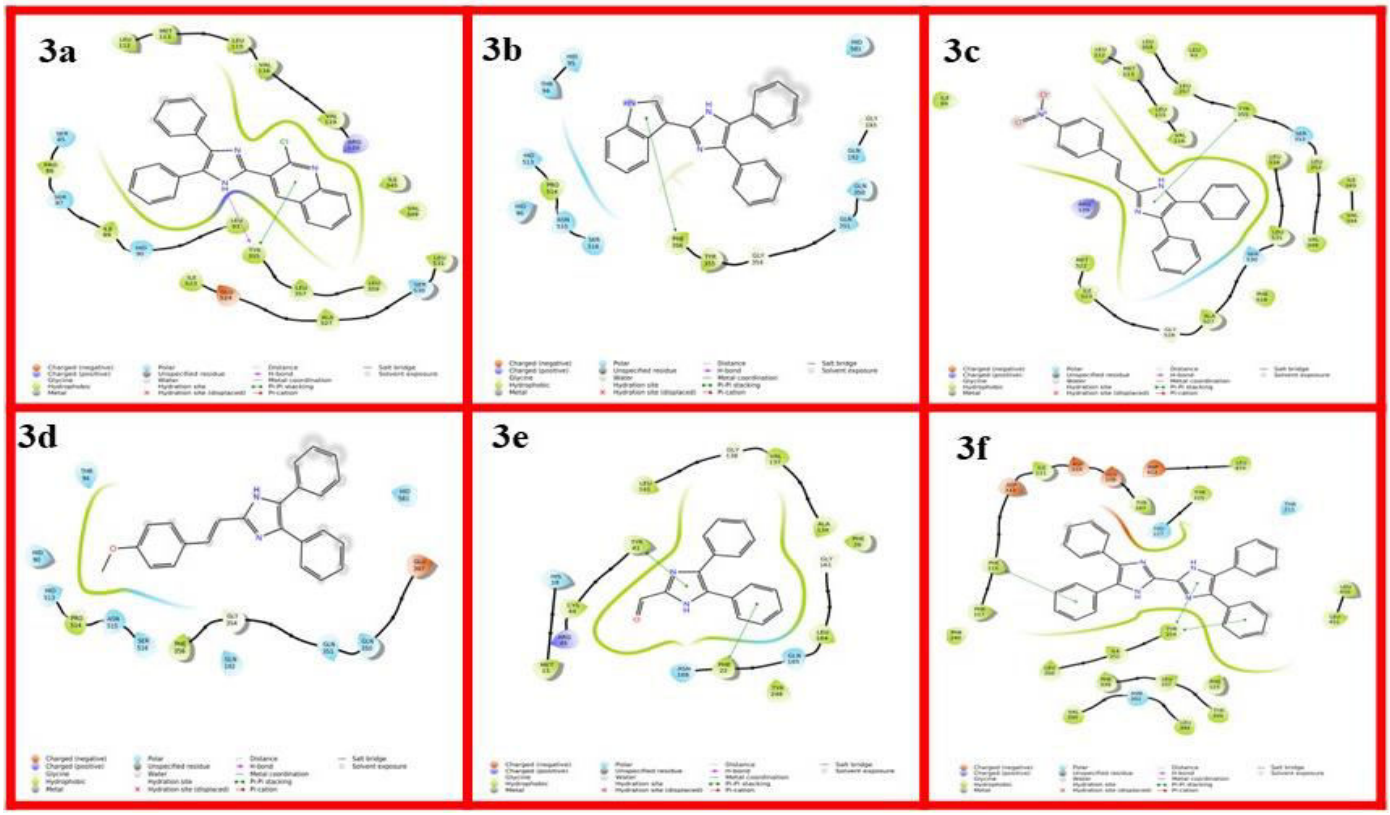

Fig. 10: Anti-inflammatory docking poses of compounds 3a-f.

Table 12: binding/docking energy values

Compound	Target Protein Docking Energy			
	3ACX	4TZT	1IYL	3N8Y
3a	-8.9	-9.8	-10.6	-2.9
3b	-8.5	-9.0	-10.7	-7.9
3c	-8.8	-9.5	-11.8	-5.7
3d	-8.8	-9.2	-11.6	-7.2
3e	-8.7	-7.1	-8.9	-7.2
3f	-9.9	-8.5	-12.4	1.4
CIP	-8.8	-------	-------	-------
ETH	-------	-4.6	-------	-------
CLO	-------	-------	-9.0	-------
IND	-------	-------	-------	-5.5

All the compounds along with standard were screened for their *insilico* antibacterial, antimycobacterial, antifungal, and anti-inflammatory activity against selected protein targets and the docking scores were tabulated. For anti-bacterial activity compounds were showing the same binding score as that of standard drug ciprofloxacin **(CIP)** where (**3f)** exhibiting more binding affinity, for antimycobacterial synthesized (**3a-d)** compounds having more binding affinities were shown better binding affinity than that of standard drug ethambutol **(ETH)** and in case antifungal all the compounds except (**3e)** exhibited more extraordinary binding than clotrimazole **(CLO)**, for anti-inflammatory compound (**3a)** exhibited very lesser binding affinity than standard drug indomethacin **(IND)** and (**3f)** indicated to be a non drug. Further these studies are related with DFT studies to confirm the electronic effects with biological activities.

3.5. DFT Analysis

The theoretical calculations using density functional theory (DFT) have been utilized to study molecular properties like charge analysis, reduced density gradient (RDG) analysis, along with molecular electrostatic potential surface analysis gives a clear understanding of the structure of the molecule [38-39]. The molecular orbital energies and electrostatic potential of the molecule were calculated in the ground state using DFT. The reduced density gradient and global descriptors such as chemical potential, electro-negativity, hardness, softness, and electrophilicity index were studied [40-41].

3.5.1. Theoretical calculations

The Becke's three parameter hybrid functional (B3) for the exchange part and the Lee-Young-Parr (LYP) correlation function at 6-31G (d,p) is used to perform the density functional theory calculations using *GAMESS-US* software [42]. All DFT calculations were performed in the gas phase only. The required input for the gamess software was generated using *Avogadro* [43]. The same parameters were used for the optimization structure and to calculate electronic properties. The surface potential and RDG were generated using *Multiwfn-3.8* [44], and visualized using *Visual Molecular Dynamics (VMD)* software [45].

3.5.1.1. Frontier molecular orbital (HOMO-LUMO) analysis and chemical reactivity indices

The frontier molecular orbitals (FMO) analysis is very helpful in understanding the nature of orbitals involved in chemical reactions. The FMO energy level of the compounds was computed using the DFT method at B3LYP/6-31G(d,p) level of theory in the gas phase. The surface of some important FMO's is shown in (**Fig.11)**. The energy gap between the highest occupied molecular orbital (HOMO) and lowest unoccupied molecular orbital (LUMO) was calculated for all the compounds.

The chemical reactivity parameters like chemical hardness (η), electronegativity (χ), electronic chemical potential (μ), and electrophilicity index (ω) were also calculated. The chemical hardness is given by $\eta=(E_{LUMO}-E_{HOMO})/2$ is connected with the stability and reactivity of a chemical system [46]. The electronegativity is defined as the ability to attract electrons towards it and is given by the expression $\chi=-(E_{HOMO}+E_{LUMO})/2$. The negative of the electronegativity of a molecule is determined by using an equation $\mu=(E_{HOMO}+E_{LUMO})/2$ is known as chemical potential. Parr has introduced the electrophilicity index (ω), is calculated using the electronic chemical potential and chemical hardness from the equation $\omega=\mu^2/2\eta$. The calculated values of chemical reactivity parameters for all the compounds are listed in (**Table13)**.

The structural and electronic properties of the compounds such as the highest occupiedmolecular orbital (HOMO) and the lowest unoccupiedmolecular orbital (LUMO) energies, orbital coefficients, together with the FMO energy gap for geometries were calculated to gain insight about their role in biological activity studies (**Table 13**). It is known that the ability of the molecule to accept or donor electrons can be rationalized by FMO analysis. The value of HOMO energy (EHOMO) is often associated with the electron donating ability of inhibitor molecule, which the higher

values of EHOMO is an indication of the greater ease of donating electrons to the unoccupied orbital or acceptor. On the other hand, it is important to examine the HOMO and LUMO energies for these compounds because the relative ordering of occupied and virtual orbital provides a reasonable qualitative indication of electronic properties and the ability of electron hole transport. Also, the value of LUMO energy (ELUMO) is related to the ability of the molecule to accept electrons, which the lower values of ELUMO shows the acceptor would accept electrons consequently. The energy differences of HOMO and LUMO (ΔEgap) provides a measure for the stability of the formed complex on the metal surface. The lower value of ÄE is related to the higher stability of the formed complex. The overall analysis of HOMO and LUMO energy values of the series, revealed that the EHOMO varied from-5.220 to -7.328eV, and ELUMO from1.420 to 5.181eV (**Table 13**).

Table 13: The calculated values of chemical reactivity parameters

Parameters	3a	3b	3c	3d	3e	3f
E_{HOMO} (eV)	-7.328	-6.579	-5.581	-5.520	-5.200	-5.224
E_{LUMO} (eV)	1.420	2.843	4.252	5.181	4.801	5.134
Energy gap (Δ) (eV)	8.748	9.422	9.833	10.701	10.001	10.358
Ionization energy (I) (eV)	7.328	6.579	5.581	5.520	5.200	5.224
Electron affinity (A) (eV)	-1.420	-2.843	-4.252	-5.181	-4.800	-5.134
Electronegativity (χ) (eV)	2.954	1.868	0.664	0.169	0.200	0.045
Chemical potential (μ) (eV)	-2.954	-1.868	-0.664	-0.169	-0.200	-0.045
Global hardness (η) (eV)	4.374	4.711	4.9165	5.350	5.000	5.179
Global softness (s) (eV^{-1})	0.228	0.212	0.203	0.186	0.200	0.193
Electrophilicity index (ω) (eV)	0.997	0.370	0.044	0.00266	0.0004	0.00019

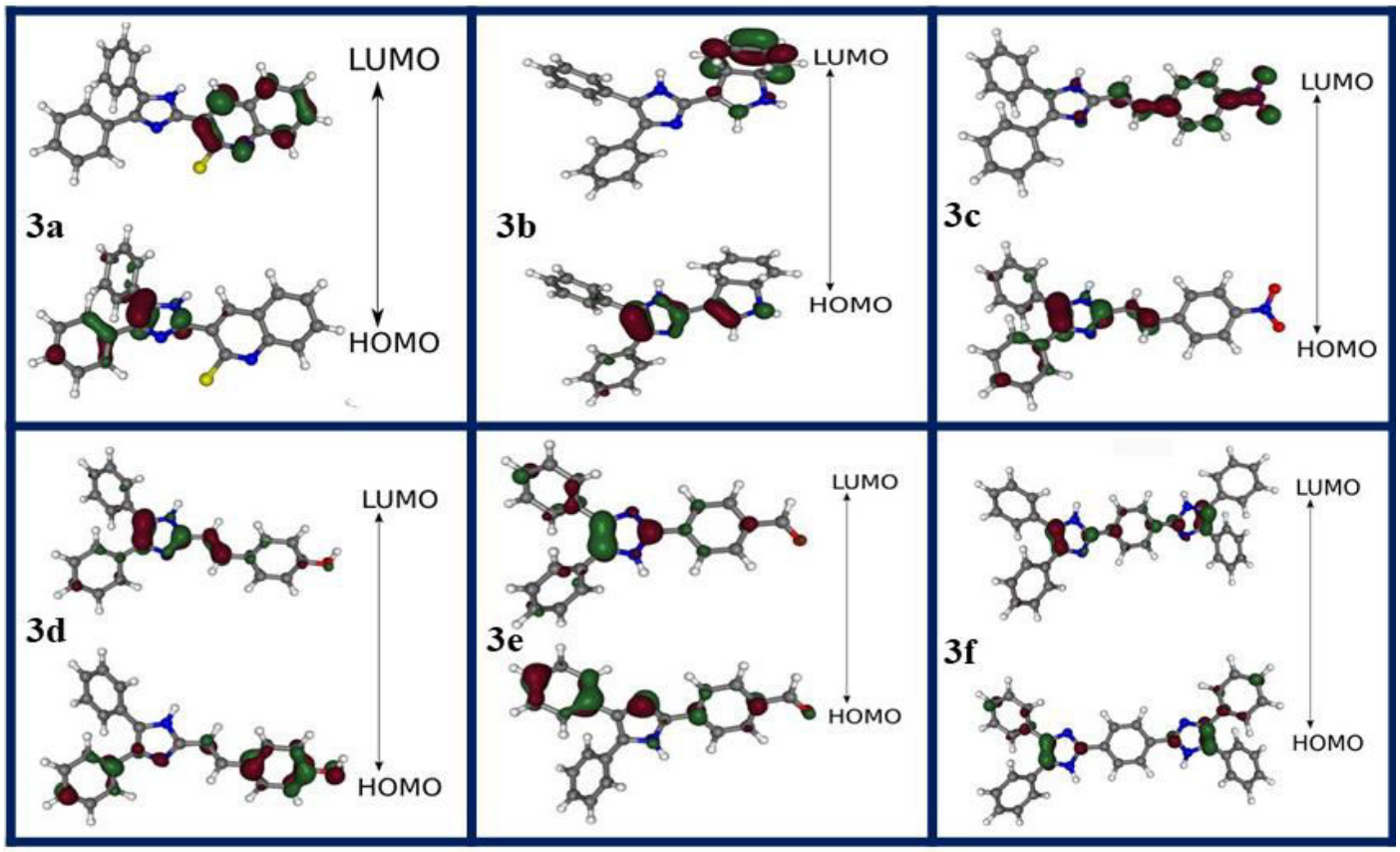

Fig. 11: HOMO-LUMO energy gap of compounds 3a-f

A set of global descriptive parameters namely, Ionization energy (I) (eV), Electron affinity (A) (eV), Electro negativity (χ) (eV), Chemical potential (μ) (eV), Global hardness (η) (eV), Global softness (s) (eV-1), Electrophilicity index (ω) (eV) alternative approach for understanding the capacity of a species to accept or donate electron. The compounds **(3d-f)** with least chemical potential (μ) value indicated that they are more nucleophile than the other. These results probably as a consequence of the substitution by the electron releasing group present. Also, have the most hardness with the highest biological activities (Docking energy values tabulated in (**Table 12)**.

3.6. Molecular electrostatic potential (MEP) analysis

Molecular electrostatic potential (MEP) or Electrostatic surface potential (ESP), also known as Electrostatic potential energy maps, decorate the three dimensional charge distributions over molecules. For the prediction of nucleophilic and electrophilic sites, ESP gives an idea of intermolecular association. MEP is a visual method to understand the polarity of the molecule. The negative electrostatic potential corresponds to an attraction of the proton by the concentrated electron density in the molecule. The positive electrostatic potential corresponds to repulsion of the proton. MEP was calculated by DFT/B3LYP at 6-31G (d,p) basis set and MEP surface plotted. An electron density is surface mapped with electrostatic potential surface display the size, shape, charge density and reactive sites of the molecules [47]. The different values of the electrostatic potential represented by color codes; red represents the regions of the most negative electrostatic potential, blue represents the region of the most positive electrostatic potential and green represent the zero electrostatic potential [48]. Mathematically, MEP can be defined as

$$V(r) = \sum_A \frac{Z_A}{|R_A - r|} - \int \frac{\rho(r')}{|r' - r|} dr'$$

where, summation ($\sum$) runs over all nuclei, Z_A is the charge of the nucleus which is located at R_A, and $\int \rho(r')$ is electron density [49]. The computed MEP using B3LYP/6-31G (d, p) level of DFT for all the compounds are shown below. The positive area of the MEP is a nucleophilic site, while the negative region is associated with an electrophilic site [50]. The potential range for compound **3a** is in the range of -48 kcal/mol to 56 kcal/mol, 3b -46 kcal/mol to 51 kcal/mol, 3c -48 kcal/mol to 46 kcal/mol, 3d -54 kcal/mol to 42 kcal/mol and the maximum distribution of surface area is in the range of -20 kcal/mol to +20 kcal/mol. The distribution of surface area based on the electrostatic potential shows a more positive potential area than the negative potential area. (**Fig.12)** shows the surface area in each ESP range of the compounds **(3a-f).**

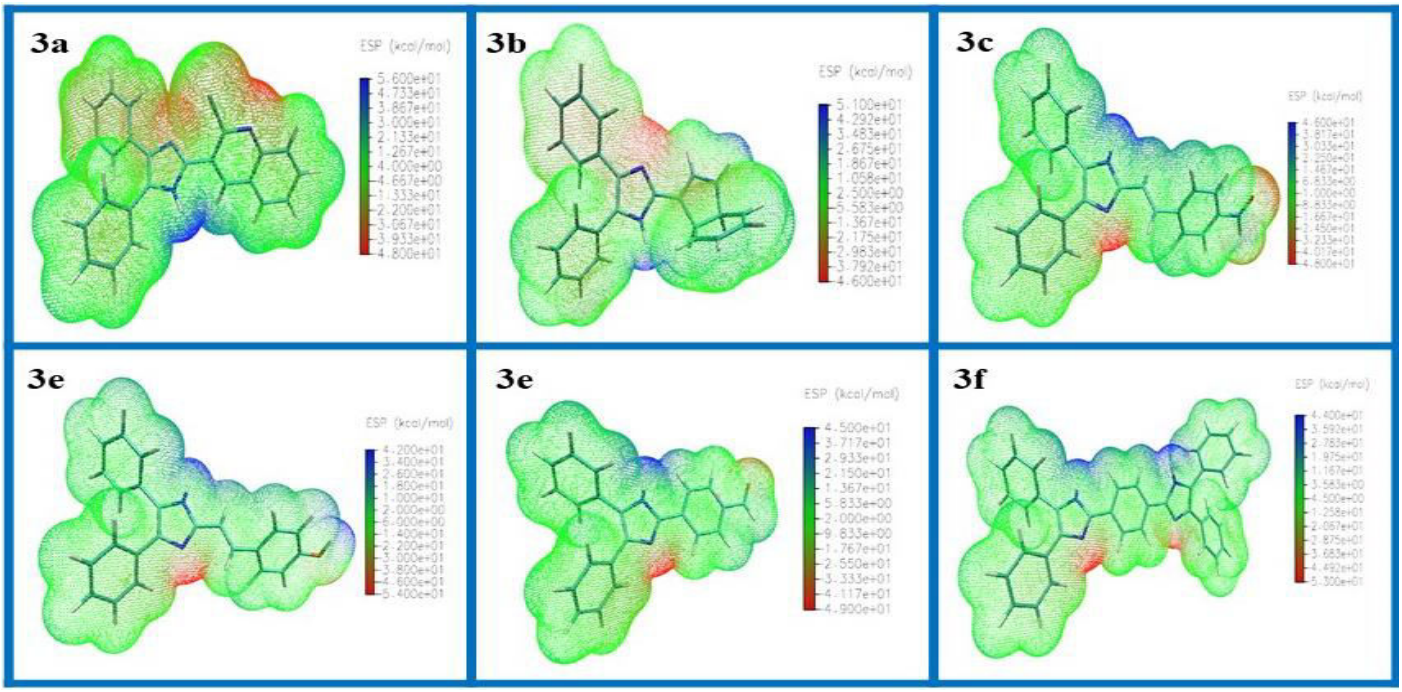

Fig. 12: Electrostatic potential surface of the compound 3a-f

3.7. Reduced density gradient (RDG)

The reduced density gradient was employed to investigate weak interaction in real space based on the electron density and its derivatives. The RDG is a dimensionless quantity obtained from electron density (ρ) and is the first derivative and is given by the equation

$$RDG(r) = \frac{\Delta\rho(r)}{2(3\pi^2)^{1/3}\rho(r)^{4/3}}$$

The weak interactions were shown in the region with low electron density and low RDG. The type of interaction can be found out with the electron density 'ρ' multiplied by the sign of λ_2 with RDG. The RDG calculations were done using *Multiwfn-3.8*. The scattered density gradient for all the compounds is shown in (**Fig.13**). The RDG versus Sign $(\lambda_2)\rho$ peaks (electron density value) gave information about the nature of interactions. Large negative values of sign $(\lambda_2)\rho$ are indicative of stronger attractive interactions, while positive ones are indicative of strong repulsion interactions. Values near to zero indicate very weak Van der Waal's interactions. The color from blue to red means from stronger attraction to repulsion, respectively. The green circles can be identified as Van der Waal (vdW) interaction region, which means that the density of electrons in these regions is low [50-51].

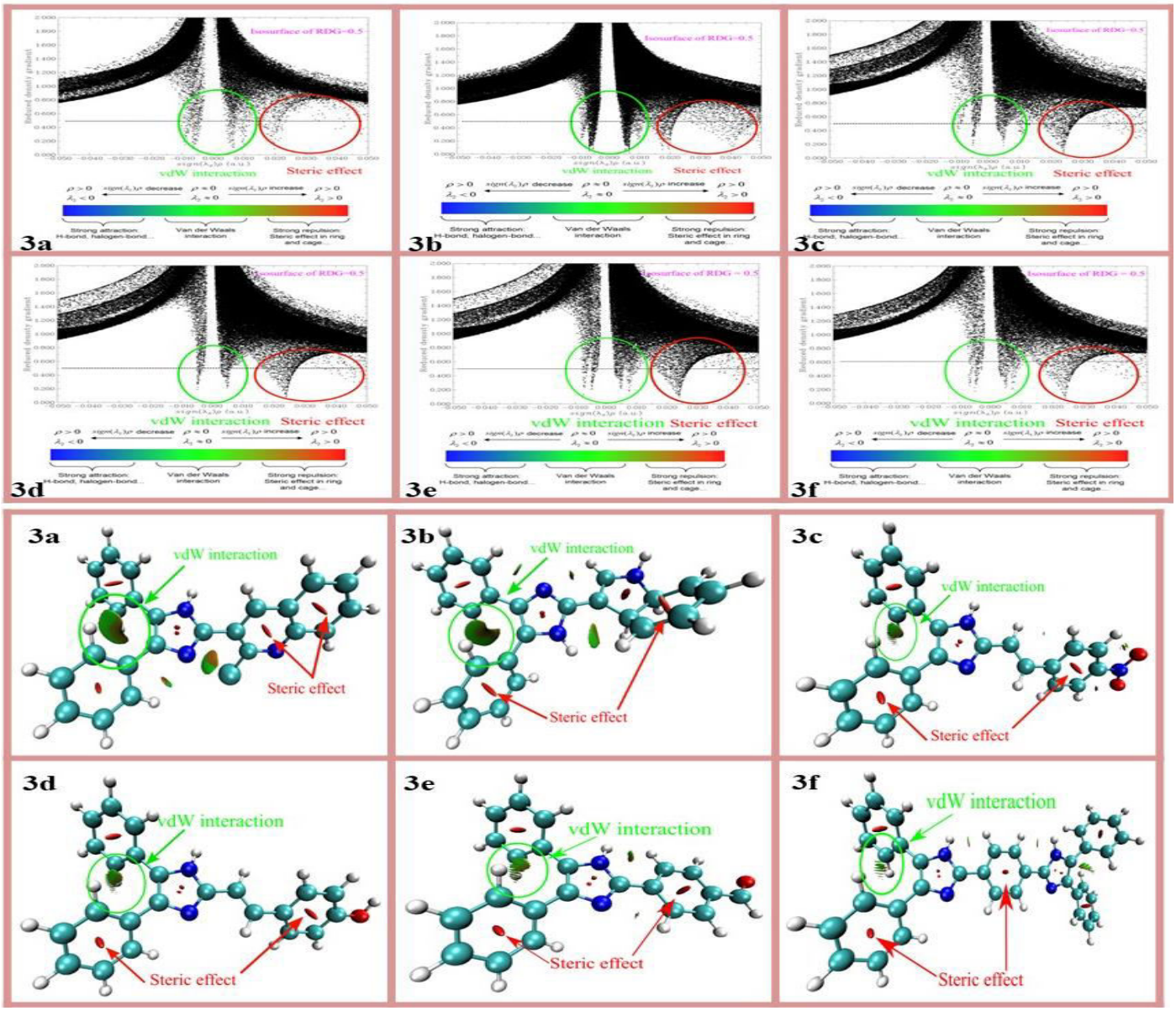

Fig. 13: Plots of the RDG versus the electron density ρ multiplied by the sign (λ_2) for compounds 3a-f and The colored surfaces of compound 3a-f according to values of sign (λ_2).

4. CONCLUSION

In the present study, we have successfully prepared a series of 2-substituted 4,5-diphenyl-1H-imidazole derivatives **(3a-f)**via one pot Debus-Radziszweski multi component condensation reaction using molecular iodine as a catalyst with high yield. The structures of the compound were established based on the physicochemical and spectral means. Further, in order of reducing the risk of failures during the early stage of drug development, ADMETox and molecular docking studies were carried out. Finally, electronic properties such as electrostatic surface potential, frontier molecular orbital and reduced density gradient were also studied and which makes way for the further investigation and development.

5. ACKNOWLEDGEMENTS

The authors are thankful to Tumkur University, Tumakuru for providing the laboratory facility to carry out this research/dissertation work and Department of Physics University of Mysuru to carry out computational studies

Conflict of interest

The authors declare that there is no conflict of interest regarding the publication of this article.

6. REFERENCES

1. Bellina F, Cauteruccio S, Rossi R.*Tetrahedron,* 2007; **63**:4571-4624.
2. Brand-Williams W, Cuvelier ME, Berset C. *Food Sci. Tech*, 1995; **28**:25-30.
3. Clark NG, Cawkill E. *Tetrahedron Lett.,* 1975; **16**:2717-2720.
4. Cozzi P, Carganico G, Fusar D, Grossoni M, et al.*J. Medi. Chem.*, 1993; **36:**2964-2972.
5. Steinman RA, Brufsky AM, Oesterreich S.*Syn. Comm.,* 2012; **14:**213-221.
6. Mishra R., Ganguly S., *Med. Chem. Res.* 2012; **21:**3929-3939.
7. BurnierM, Wuerzner G., *Drug Metab. Toxicol.,* 2011; **7:**643-649.
8. Ali I, Lone M. N, Aboul-Enein H Y, *Medchem. Comm.,* 2017; **8:**1742-1773.
9. Pattan SR, Reddy VVK, Manvi FV, Desai BG, Bhat AR. *Indian J. Chem.,* 2006; **45B:**1778-1781.
10. Gupta P, Hameed S, JainR,.*Eur. J. Med. Chem.*, 2004; **39:**805-814.
11. Vinggaard AM, Hass U, Dalgaard M, Andersen HR, et al., *Int. J. Androl.*, 2006; **29(1):**186-192.
12. Astruc D, Boisselier E, Ornelas C, *Chem. Rev.,* 2010; **110**:1857-1959.
13. Singh R, Ahmad M, Bharadwaj PK, *Crystal Growth & Design,* 2012; **12**:5025.
14. Schmierer R, Mildenberger H, Buerstell H, Ger. Pat. 361436, *Chem. Abstr.*, 1987; **88**:37838.
15. Zhang M, Li M, Li F, Cheng Y, Zhang J, Yi T, Huang C, *Dyes Pigm.,* 2008; **77**:408-414.
16. Saravanan K, Srinivasan N, Thanikachalam V, Jayabharathi J. *J. Fluoresc,* 2011; **21:**65-80.
17. Jayabharathi J, Thanikachalam V, Devi KB. *Biomol. Spectrosc.*, 2011; **82**:513-520.
18. Mukherjee S, Weyhermuller T, Bill E, Chaudhuri P. *Euro.J. Inorg. Chem.*, 2004; 4209.
19. Fern′andez R, Ramos JA, Esp′osito L, Tercjak A, Mondragon I. *Macromolecules*, 2011; **44(24):**9738-9746.
20. Nishihara H, *Coord. Chem. Rev.*, 2005; **249:**1468.
21. Bianchi A, Delgado-Pinar E, Giorgia C, Pina F,Garc′ıa-Espa˜na E. *Coord.Chem. Rev,* 2014; **260**: 156-162.
22. (a) Breslin HJ, Miskowski TA, Rafferty BM, Coutinho SV, Palmer JM,et al. *J. Med. Chem.,* 2004; **47**:5009. (b) Baldwin JJ, Engelhardt EL, Hirschmann R, et al.*J. Med. Chem.,* 1979; **22:**687. (c) James DS,Fanta PE.*J. Org. Chem.,* 1962; **28:**390.
23. (a) Curtis NJ, Brown RS.*J. Org. Chem.*, 1980; **45:**4038. (b) Oliver JE, Sonnet PE.*J. Org. Chem.,* 1973; **38:**1437. (c) Wolkenberg SE, Wisnoski DD, Leister WH, Wang Y, Zhao ZJ, LindsleyCW. *Org. Lett.*, 2004; **6:** 1453. (d) Baldwin JJ, Christy ME, Denny GH, Habecker CN, et al.*J. Med. Chem.,* 1986; **29:**1065.
24. Susan EB, Viscount D, Dhanesh GC, Denis MG.*J. Chem. Soc.*, 1987; 639-643.
25. (a) Weidenhagen R,RienackerH.*Ber.*, 1939; **72:**57. (b) Weidenhagen R. HerrmannR.*Ber.*,1935;**68:** 2205. (c)Weidenhagen R, HerrmannR.*Angew. Chem.,* 1935; **48:**596.
26. Baldwin JJ, Lumma PK, Novello FC, Ponticello GS, Sprague JM, Duggan DE. *J. Med. Chem.,* 1977; **20:**1189.
27. Yi-Ming Ren, Chun Cai, Ren-Chun Yang, *RSC Adv.,* 2013; 3:7182-7204.
28. Arshia P, Md. Rafi Sk. A, Kabeer AS, Sudhir D P, Rajendra PP. *ARKIVOC*, 2007; 12-18.
29. Gopalan S, Kalieswaran Va, Thangaraj A, Jayaraman A, Easwaran M, et al. *Chemistry Select,* 2018; **3:**3680-3686.

30. Chakrabhavi DM, Srinivasa V, Shobith R, Lewis M, et al. *PLoS ONE*, 2016;**11(4):**e0153155.
31. Karnambaram A, Margarita C, Paulina C, Rodrigo Ramos-Hernández, Venkatesan P, et al. *Chemistry Select,* 2020; **5:**415-425.
32. Hariharasubramanian A, Ravichandran D. *RSC Advances,* 2014; **4(97)**:54740-54746.
33. Daina A, MichielinO, Zoete V. *Sci. Reports*, 2017; **7**:42717.
34. Jie Dong, Ning-Ning Wang, Zhi-Jiang Yao, Lin Zhang, Yan Cheng, et al. *J. Cheminf*, 2018; **10**:29
35. Krishna Swamy G. Ph.D. Thesis, Tumkur. Univ. (2018)**.**
36. Rodolpho BC, Vinicius AM, Meryck Silva FB, et al. *Mol. Inf.,* 2015; **34:**698-701.
37. Lipinski CA. *Drug Discov. Today Technol.,* 2004; **1:** 337-341.
38. Maiti A, Svizhenko A, Anantram MP, *Phys. Rev. Lett.*, 2002; **88:**1268051-1268054.
39. Zhou D, Ma D, Wang Y, Xianchun L, Xinhe B, *Chem. Phys. Lett.,*2003; **373**:46-51.
40. Leconte J, Markovits A, Skalli MK, Minot C, Belmajdoub A.*Surf. Sci.,* 2002; **497**:194-204.
41. a)Toy M, Tanak H.*Spectrochimic. Acta A.,* 2016; 152:530-536. b) Raj RK, Gunasekaran S, Gnanasambandan T, Seshadri S, *Spectrochimic. Acta A.,* 2015; **139**:505-514. c) Diwaker CS, Kumar C, Kumar A, Chandraju S, *Spectrochimic. Acta A.*, 2015; **150:** 602-613.
42. Gandhimathi S, Balakrishnan C, Theetharappan M, Neelakanthan MA, Venktaraman R, *Spectrochimic. Acta A.,* 2017; **175:**134-144.
43. Geetha DV, Fares HA, Yasseir HEM, Sridhar MA, Shaukath AK, Lokanath NK. *J. Mol. Str.*2019; **1178:**384-393.
44. Barca GMJ, Bertoni C, Carrington L, Datta D, De Silva N, et al. *J. Chem. Phys.,* 2020; **152:**154102.
45. Hanwell MD, Curtis DE, Lonie DC, Vandermeersch T, Zurek E, Hutchison GR. *J. Cheminform,* 2012; **4:**17
46. Lu T, Chen F.*J. Comput. Chem.*, 2012; **33:**580-592.
47. Humphrey W, Dalke A, Schulten K. *J. Molec. Graphics,* 1996; 33-38.
48. Parr RG, Donnelly AR, Levy M, Palke WE. *J. Chem. Phys.*1978; **68**.
49. Itskowitz P, Berkowitz ML.*J. Phys. Chem. A.,* 1997; **101:**5687-5691.
50. Lu T, Chen F, *J. Mol. Graph. Model*, 2012;**38**:314-323.
51. Johnson ER, Keinan S, Mori-Sanchez P, Contreras-Garcia J, Cohen AJ, Yang W. *J. Am. Chem. Soc.*, 2010; **132:**6498-6506.